on the sky plane is shown in each case. Tails from individual fragments could be resolved up to about 10 arcsec. An ambient dusty region extending to about 30 arcsec on the anti-sun direction of the cometary train is evident on all the frames. At the comet's distance this equals a projected linear distance of about 120,000 km.

A comparison of the image of SL9 with that on 29 May 1993, shows that the morphology of the dusty region surrounding SL9 drastically changed[7]. For example, the dust envelope has significantly thinned and the wings extending on either side of the train are missing. The dynamics of the dust in the tail of the comet SL9 is complicated. For normal comets which develop tails while approaching the Sun, the syndynes and synchrones[8] can be determined entirely from the grain sizes, their density and optical properties. This is so because the ratio of the radiation pressure force to the gravitational force depends only on the comet's heliocentric distance. In case of SL9, while the radiation pressure on a grain of given size and density is very nearly the same, the gravitational force which is governed by three-body dynamics is not. Analysis of the tail structure to derive information on the nature of the grains and their size distribution or to look for evidences of bursts or jets requires detailed modelling[9]. The limited data obtained on two successive days precludes such an attempt.

1. I A.U C. No. 5725, 1993.
2. I.A.U.C. No. 5730, 1993.
3. Jewitt, J., Luu, J. and Chen, J., *Bull. Am. Astron. Soc.*, 1993, **25**, 1042.
4. I A.U.C. No. 5906, 1993.
5. Lasker, B. M., Sturch, C. R., McLean, B. J., Russell, J. L., Jenkner, H. and Shara, M. M., *Astron. J*, 1990, **99**, 2019–2058.
6. Yeomans, D. K. and Chodas, P. W., 1993, private communication (orbit ref. 12/17/93)
7. Kameswara Rao, N, Mayya, Y. D., Eswar Reddy, B. and Prabhu, T. P., *Bull. Astron Soc. India*, 1993, **21**, 221–222.
8. Finston, M. F. and Probstein, R. F., *Astrophys. J.*, **154**, 327–352.
9. Finston, M. F. and Probstein, R. F., *Astrophys. J.*, **154**, 353–380.

ACKNOWLEDGEMENTS. This work was supported in part by funding from the Department of Science and Technology, Government of India, and the Smithsonian Institutes, Washington.

Received 1 July 1994, revised accepted 1 October 1994

Burst vortex flow-field on a delta wing—A numerical simulation using Euler equations

Anand Kumar
Computational and Theoretical Fluid Dynamics Division, National Aerospace Laboratories, Bangalore 560 017, India

A numerical simulation of vortex breakdown on a delta wing is carried out. Flow-field within and around vortex breakdown is presented to illustrate the vortex breakdown phenomenon.

WHEN a delta wing is placed in a flow at an incidence, flow separates along the leading-edge and vorticity is shed, which rolls up to form coiled vortex sheets above the wing, with a core of high vorticity. The suction in the vortex core induces additional lift which is exploited aerodynamically, as in the design of modern fighter aircraft. An increase in the incidence leads to a stronger vortex. If the vortex is sufficiently strong, a sudden change in the structure of the vortex core, known as vortex breakdown or vortex bursting, occurs somewhere along the vortex axis. Vortex breakdown is characterized by a sudden drop in suction and a pronounced alteration of velocity field in the vortex core. The two types of vortex breakdown that occur on delta wings are called bubble type and spiral type. Due to its importance in aeronautical and non-aeronautical applications, vortex breakdown, first observed by Peckham and Atkinson[1], is an active area of experimental and theoretical research. A recent review of vortex breakdown is presented by Delery[2].

Even after three decades of research, the underlying mechanisms leading to vortex breakdown are still not well understood, although several theories of vortex breakdown have been proposed[3]. Here, based on Euler equations, numerical simulation of burst vortex flow-field over a sharp leading-edge delta wing is carried out, with the hope that some of the observations made here will help understand the vortex breakdown mechanisms better. The vortex breakdown phenomenon is highlighted by presenting the computed flow-field. The use of Euler equations for our study of vortex breakdown is based on the experimental observations[4] that the vortex breakdown is almost independent of viscous effects. We consider a sharp leading-edge wing since the primary separation is then fixed along the leading-edges. The vortex sheet shed from the sharp leading-edge which rolls up to form the primary vortex is well modelled

by the Euler equations. The secondary vortex that is not modelled by the Euler equations, displaces the primary vortex slightly upward and inboard, and does not play a role in the breakdown process.

The sharp leading-edge delta wing considered has an aspect ratio 1.6 (leading-edge sweep of 68.2°) and is placed at an incidence of 30° to the free-stream. The geometrical details of the wing are the same as in the experiment of Hummel and Srinivasan[5]. A multi-block grid[6] having 279 K grid points is used. Euler equations are solved using a finite-volume scheme for spatial discretization, explicitly added artificial dissipation and a Runge–Kutta scheme with acceleration devices for time integration[7]. Results presented here have been obtained for a Mach number of 0.3. The computing time is about 90 h on the four processor Flosolver at the CTFD Division, NAL. Some features of the simulated vortex breakdown are presented below.

The computed vortex breakdown is illustrated by particle traces shown in Figure 1. In this figure, particles are released close to the vortex axis, near the apex. They travel along the vortex axis till about the midchord where they abruptly depart from the vortex axis. This qualitative change in the character of the vortex is referred to as vortex breakdown. The figure also shows a trace of a particle released from a point downstream of the breakdown. The particle travels backward and forward before escaping the burst flow region. Computed pressure coefficient and axial velocity along the vortex axis are shown in Figure 2. The figure shows that a sudden drop in the vortex suction occurs around midchord and the flow along the vortex axis slows down rapidly due to vortex breakdown.

By an examination of the computed flow-field on each transverse grid plane, it is determined that the vortex breakdown occurs at the grid plane at $x = 0.501$. The streamwise velocity contours in the transverse grid plane at the breakdown are shown in Figure 3. The velocity contours show formation of a 'stagnation' region where the flow slows down more rapidly than the surrounding fluid resulting in a minima of the streamwise velocity. This stagnation region or deficit velocity region grows in the downstream direction and a flow reversal

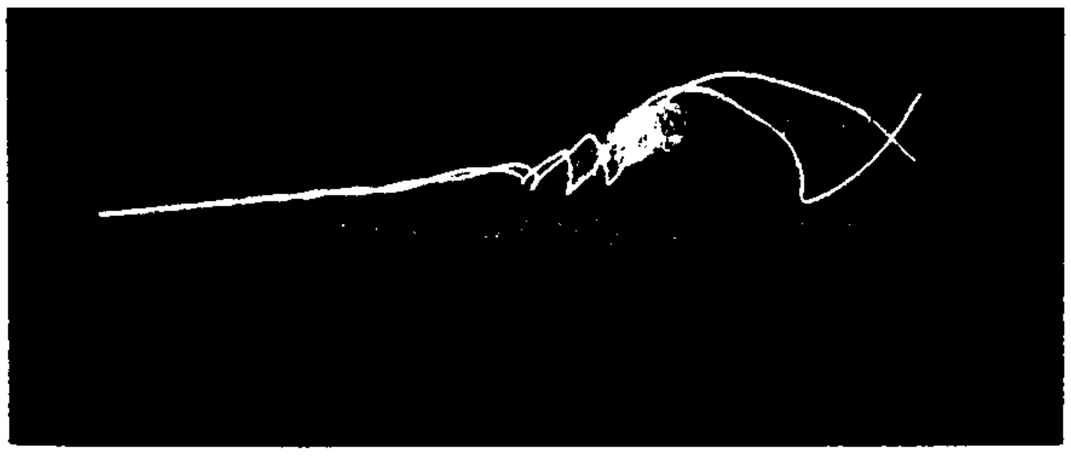

Figure 1. Particle traces showing vortex breakdown.

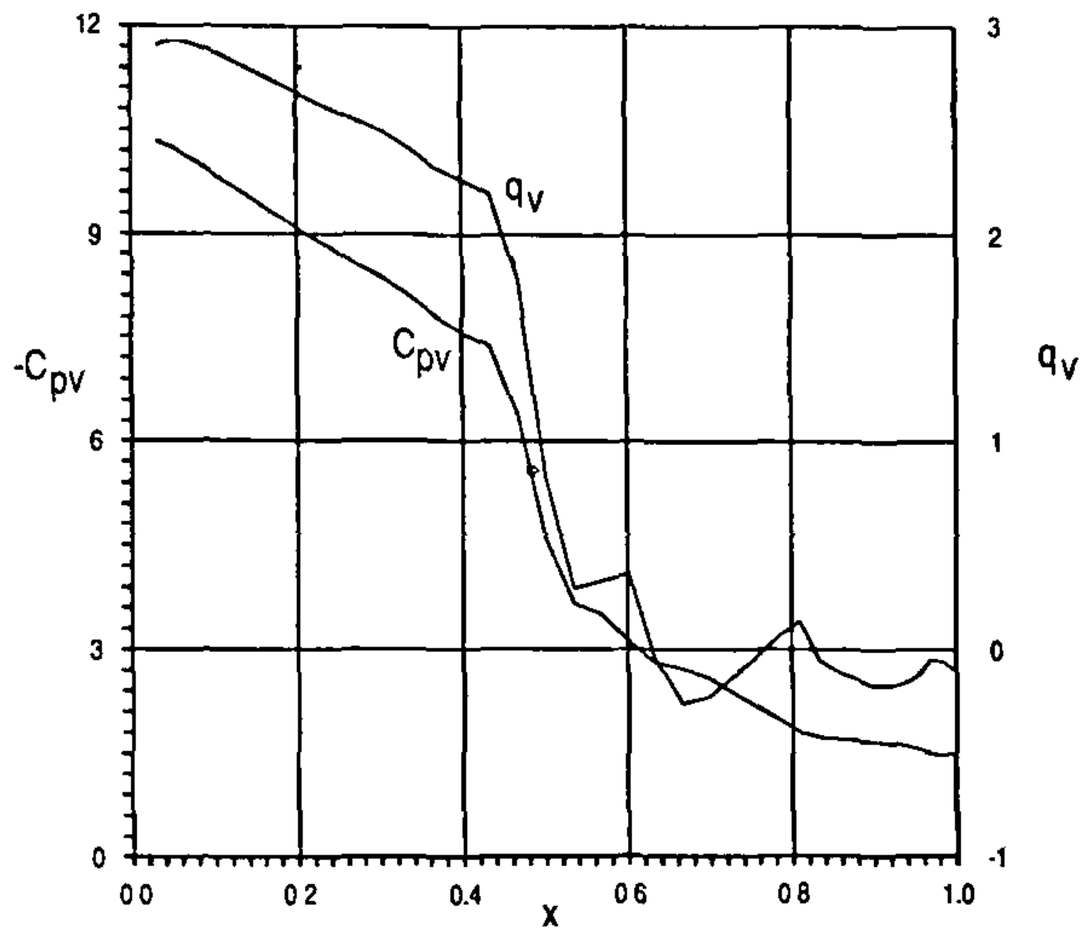

Figure 2. Pressure coefficient and axial velocity along the vortex axis

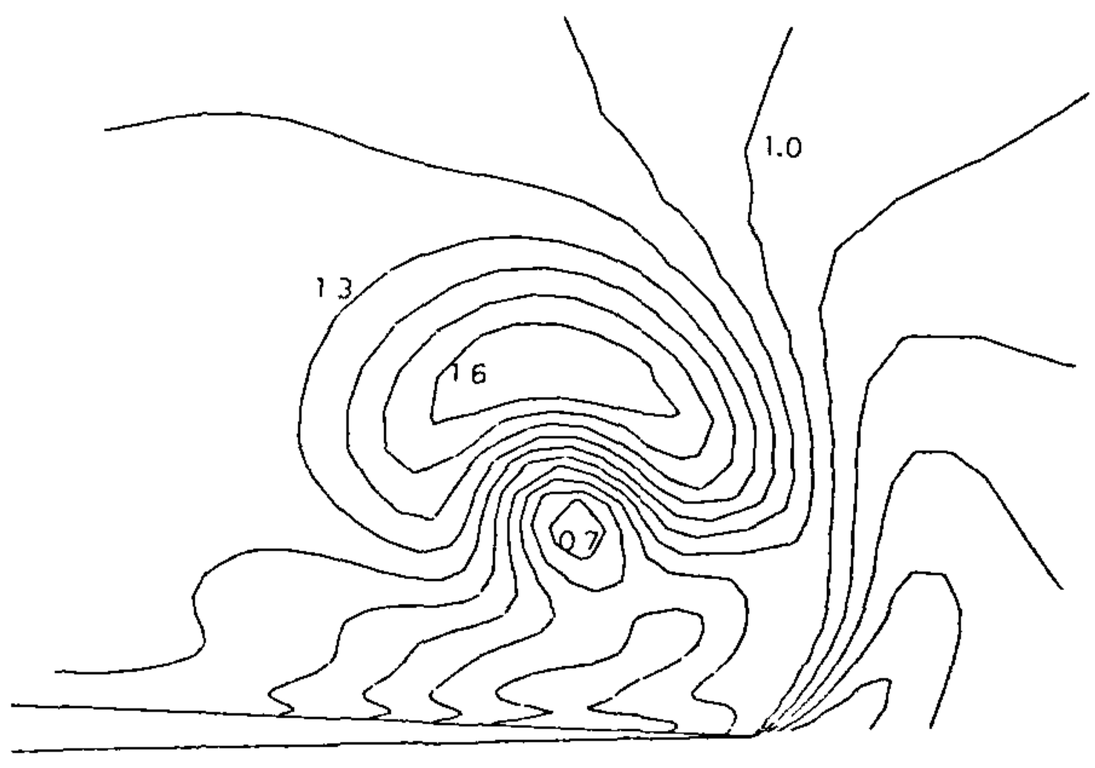

Figure 3. Contours of streamwise velocity at the breakdown, $x = 0.501$.

occurs in the core. Payne *et al.*[8] using a seven hole probe, have given the velocity survey at the breakdown on a 70° delta wing at 30° incidence, which is shown here in Figure 4. A stagnation region at the breakdown is also seen in their experiment. Hummel[9] has also reported a stagnation region in his five hole probe measurements of the vortex breakdown on a 79° delta wing at 31° incidence. There is a good similarity between the computed (Figure 3) and the experimental velocity field (Figure 4) at the breakdown. The process of breakdown as captured in the computation is thus similar to that in the experiment.

The transformation of the vortex core from a jet-like flow to a wake-like flow due to the breakdown is seen

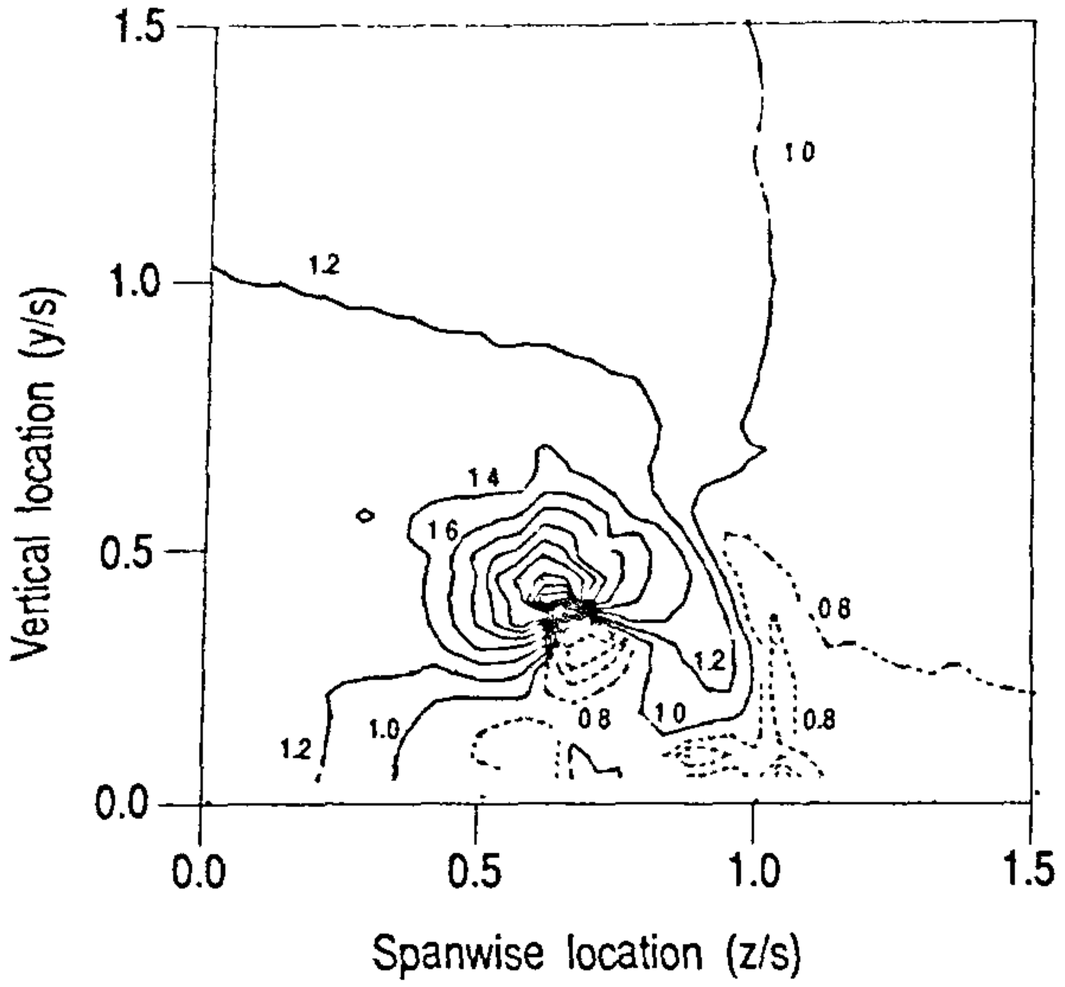

Figure 4. Streamwise velocity survey on a 70° delta wing at 30° incidence, $x = 0.5$ (ref. 8).

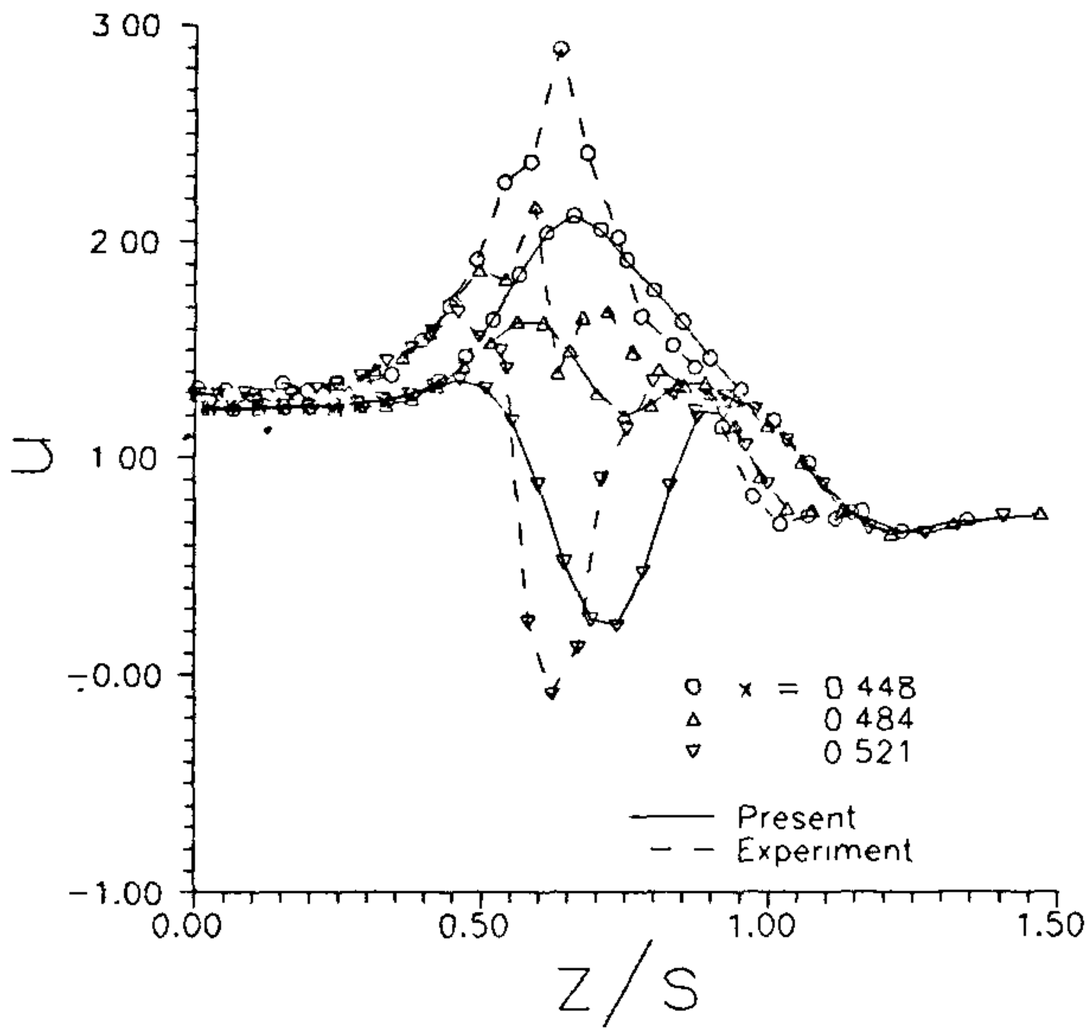

Figure 5. Computed streamwise velocity in the vortex core showing transformation from a jet-like flow to a wake-like flow due to vortex breakdown and its comparison with the experimental measurements of ref. 10.

from Figure 5, where the computed streamwise velocity profiles on the line through the vortex axis and parallel to the wing are shown for different streamwise locations. The figure also shows the LDA measurements of Iwanski[10], which is for a 70° delta wing at 30° incidence. The computed development of the flow through the

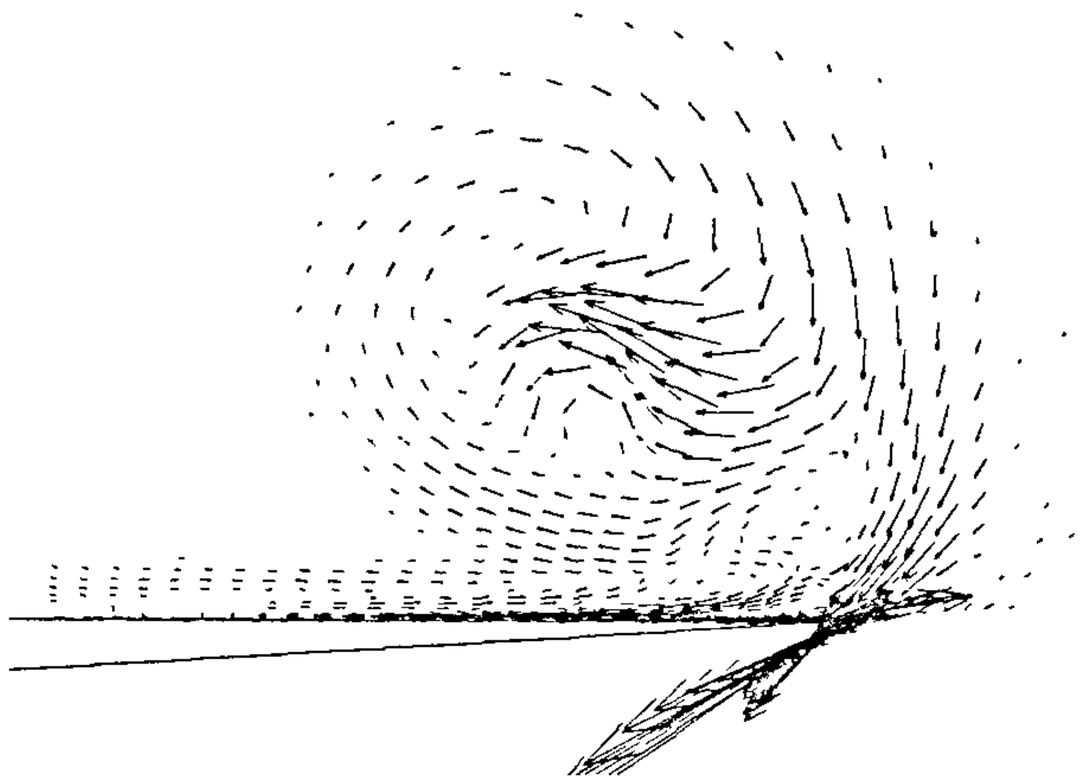

Figure 6. Vorticity vectors in the transverse plane at the breakdown.

vortex breakdown is seen to be similar to that in the experiment. The computed vortex is outboard of that in the experiment due to the absence of the secondary vortex in the Euler solution. The flow reversal along the vortex axis and the velocity profiles in the vortex core show that the computed vortex breakdown for the flow conditions considered is of bubble type.

Before the breakdown, the computed vorticity vectors close to the vortex axis are predominantly along the axial direction and are spiralling such that the azimuthal vorticity is positive. They suddenly tilt at the breakdown, thereby reducing the axial vorticity considerably and giving rise to negative azimuthal vorticity. Figure 6 shows the vorticity vectors in the transverse plane at the breakdown, where the formation of negative azimuthal vorticity due to breakdown can be seen. Negative azimuthal vorticity in the breakdown region has also been experimently observed by Iwanski[10]. According to Brown and Lopez[11], the physical mechanism of vortex breakdown relies on the production of negative azimuthal vorticity.

In conclusion, vortex breakdown on a sharp leading-edge delta wing of aspect ratio 1.6 at 30° incidence is presented. The computed vortex breakdown is of bubble type. At the breakdown, a stagnation region develops which grows as one moves downstream and a flow reversal occurs in the vortex core. A sudden tilting of the vorticity vectors close to the vortex axis occurs at the breakdown leading to a large reduction in axial vorticity and production of negative azimuthal vorticity. Vortex breakdown leads to a sudden drop in the vortex suction and the jet-like flow in the vortex core transforms to a wake-like flow. The computed burst vortex flow-field is similar to that observed in the experiment. The present study also shows that the vortex breakdown mechanisms at high Reynolds number can be computed within the

framework of the Euler equations. It is planned to make a detailed presentation of the results in a CFD journal.

1. Peckham, D. H. and Atkinson, S. A., Preliminary results of low-speed wind tunnel tests on Gothic wing of aspect ratio 1.0, ARC C.P. No. 508, T.N. No Aero 2504, 1957.
2. Delery, J. M., *Prog Aerosp. Sci*, 1994, **30**, 1–59.
3. Mudkavi, V. Y., *Proceedings of the Fluid Dynamics Symposium in honour of Prof. R. Narasimha*, NAL SP 9315, 1993, 123–135, National Aerospace Laboratories, Bangalore.
4. Erickson, G. E., Vortex flow correlation, AFWAL-TR-80-3143, 1980, Roos, F. W. and Kegelman, J. T, AIAA paper 90-0383, 1990.
5. Hummel, D. and Srinivasan, P. S., *J. R. Aero. Soc.*, 1971, **71**, 319–322.
6. Kumar, A. and Sudharsan, R., *J. Comp. Fluid Dyn.*, 1995 (in press).
7. Kumar, A., *Proceedings of the Fluid Dynamics Symposium in honour of Prof. R. Narasimha*, NAL SP 9315, 1993, 77–89, National Aerospace Laboratories, Bangalore.
8. Payne, F. M., Ng, T. T. and Nelson, R. C., AIAA paper 87–1231, 1987.
9. Hummel, D., *Z. Flugwiss*, 1965, **13**, 158–167.
10. Iwanski, K. P., Masters Thesis, Univ. of Notre Dame, Notre Dame, Indiana, 1988, as reported in Ng, T. T., Nelson, R. C. and Payne, F. M., AGARD CP 437, 1988, 11 1-11.13; Nelson, R. C. and Visser, K. D., AGARD CP 494, 1990, 21.1-21 15.
11. Brown, G. L. and Lopez, J. M., *J. Fluid Mech.*, 1990, **221**, 553–576.

Received 28 September 1994; revised accepted 23 November 1994

A possible relationship between the wind in the atmospheric boundary layer over north Indian Ocean and the summer monsoon rainfall over India

O. P. Singh

India Meteorological Department, Shivajinagar, Pune 411 005, India
Present address: Meteorological Unit, Civil Aviation Training College, Bamrauli, Allahabad 211 002, India

The relationship between the power of wind in the atmospheric boundary layer over the north Indian Ocean and the summer monsoon rainfall over India has been studied utilizing marine meteorological data for the north Indian Ocean and all-India rainfall for the period 1972–91. Monthly mean fields of wind, air temperature and sea surface temperature have been determined, and the power of wind in the atmospheric boundary layer has been computed on a grid mesh of 5° over the area bounded by 50°E to 100°E, north of the equator. Correlation coefficients were computed between seasonal (June–September) area-weighted rainfall over India and the winds in atmospheric boundary layers over the Arabian Sea and the Bay of Bengal during the month of May. Significant correlations have been found between (i) June–September rainfall over India and the wind over the Arabian Sea area bounded by the equator and 10°N during May, and (ii) June–September rainfall over India and the wind over the north Indian Ocean between the equator to 10°N and 50°E–100°E. We find that the wind in the boundary layer over the equatorial regions of the north Indian Ocean (equator to 10°N) during May could be a useful predictor for the summer monsoon rainfall.

THE quantum of rains falling over India during the summer monsoon from June to September is important for India's economy. It is thus natural that the prediction of summer monsoon rainfall should draw the attention of many meteorologists.

Pioneering efforts in this direction have been made by Blanford[1] and Walker[2]. Recently, Singh[3] and Singh and Joshi[4] have shown that the initial state of the north Indian Ocean before the commencement of summer monsoon season plays an important role in the performance of the ensuing monsoon.

This communication reports the relationship between the wind strength in the atmospheric boundary layer over the north Indian Ocean during May and all-India rainfall for the subsequent monsoon. The mechanical stirring of the ocean is dependent on the wind in the lower atmosphere. By mechanical stirring, the centre of gravity of the upper ocean is raised as the warmer surface waters are forced to subsurface layers, enhancing the heat storage capacity of the ocean. The heat storage capacity of the ocean has a major influence on climate.

The power of the wind, P (W m^{-2}), has been computed at each grid point by

$$P = \rho_a C_D [(U^2 + V^2)^{1/2}]^3, \quad (1)$$

where $\rho_a = 1.18$ kg m^{-3} is air density, C_D is the exchange coefficient for momentum, U and V are the eastward and northward components of the wind velocity in m S^{-1}. For this study C_D is considered to be a function of wind speed, $(U^2 + V^2)^{1/2}$, and of the difference between air and sea temperatures, $T_a - T_s$. It is given by[5]

$$\begin{aligned} C_D = {} & 0.934 \times 10^{-3} + 0.788 \times 10^{-4} (U^2 + V^2)^{1/2} \\ & + 0.868 \times 10^{-4} (T_a - T_s) - 0.616 \times 10^{-6} (U^2 + V^2) \\ & - 0.120 \times 10^{-5} (T_a - T_s)^2 - 0.214 \times 10^{-5} \\ & \times (U^2 + V^2)^{1/2} \ (T_a - T_s). \end{aligned} \quad (2)$$